Asian Journal of Chemistry; Vol. 35, No. 7 (2023), 1616-1624

ASIAN JOURNAL OF CHEMISTRY

https://doi.org/10.14233/ajchem.2023.27921

# Synthesis, Biological Evaluation, DFT Studies and Molecular Docking of Novel 4-(5-(1*H*-Imidazol-1-yl)-3-methyl-1-phenyl-1*H*-pyrazol-4-yl)-6-amino-3-methyl-1-phenyl-1,4-dihydropyrano[2,3-*c*]pyrazole-5-carbonitrile and its Derivatives

RAJAT PATEL[1,*], PUJA SHARMA[1], ROHIT R. KOSHTI[1], AKSHAY VYAS[1] and CHETAN B. SANGANI[2,*]

[1]Shri Maneklal M. Patel Institute of Sciences & Research, Kadi Sarva Vishwavidyalaya, Gandhinagar-382024, India
[2]Department of Chemistry, Government Science College, Sector 15, Gandhinagar-382016, India

*Corresponding authors: E-mail: rajatmsc93@gmail.com; chetansangani1986@yahoo.com

*Received*: 22 April 2023; *Accepted*: 18 May 2023; *Published online*: 6 July 2023; AJC-21283

A novel series consisting of eight imidazol-pyrazole hybrids ( **9a-h**) are synthesized using a base catalyzed one pot multi-component reaction (MCR) and screened for *in vitro* biological activities. All compounds were found to display high biological activities but compound **9g** was found to be the most active against EGFR ($IC_{50}$ of 0.11 ± 0.02 µm), A549 and HepG2, while compound **9h** was found to be most active against FabH ($IC_{50}$ of 2.6 µm) *E. coli*. The DFT studies and molecular docking was done for compounds **9a-h** to calculate the distance and angle between the active parts of the molecules and charge density over the molecules affecting the binding of molecules in the active pockets with greater binding affinity.

**Keywords: Imidazole-pyrazole hybrid, Active pockets, Biological activities, DFT studies, EGFR, FabH.**

## INTRODUCTION

One of the most important roles of medicinal chemistry is in finding new bioactive molecules, their structure elucidation, therapeutic behaviour and action mechanism [1]. Further new threats due to the emergence and diffusion of multi drug resistant bacteria have again emphasized the need for the emergance of new bioactive molecules [2,3]. Studies suggest that heteroatoms like nitrogen, sulphur, oxygen constitute more than 85% of biological active moieties [4]. Nitrogen containing heterocycles are of great importance as they are a part of pharmaceuticals products as anticancer, antidepressive, antifungal and antibacterial agents and are an essential constituent of several biologically important molecules like vitamins, nucleic acids and dyes [5,6].

Among the five membered nitrogen containing heterocyclic compounds, pyrazole and imidazole motifs have shown promising biological activities in the field of medicinal and pharmaceutical chemistry [7,8]. Pyrazole moieties possess excellent anticancer [9], antibacterial [10], anti-inflammatory [11], antifungal [12] and analgesic activities [13], *etc*. Studies also show that the pyrazoles along with other heterocyclic compounds act as potent anticancer agents targeting EGFR tyrosine kinase and FabH [14-17].

Also, imidazole is known to exhibit excellent pharmacokinetic properties and is also present in various natural products like purines, nucleic acids and histamines [8]. Imidazole displays excellent anticancer activity [18] and therefore provides new areas in the designing of new anticancer drugs along with several new pharmacophores. Finally, from the molecular design point of view, combining two such promising pharmacophores into one single unit using one pot multicomponent reaction (MCR) was considered in the given study. The excellent biological activities of both pyrazole and imidazole were taken into consideration while carrying out the current study. In the present work, we have tried to synthesize a new antimicrobial moiety by combining pyrazole and imidazole derivatives and did the biological evaluation for any significant changes and carried out DFT studies and molecular docking for the same. Herein, the synthesis, biological evaluation, DFT studies and molecular docking of novel 4-(5-(1*H*-imidazol-1-yl)-3-methyl-1-phenyl-1*H*-pyrazol-4-yl)-6-amino-3-methyl-1-phenyl-1,4-dihydropyrano[2,3-*c*]pyrazole-5-carbonitrile and its derivatives using one pot MCR approach is reported.

## EXPERIMENTAL

All the chemicals were purchased commercially and used as such. Solvents like DMF and ethanol used were of analytical grade. Potassium carbonate and pyridine were used as catalyst in the synthesis route. TLC was carried out to closely monitor all the steps. Elemental analysis (% C, H, N and O) was done with the help of CHN/S/O elemental analyzer 2400 Series II, Perkin-Elmer. A mass spectrum for all the synthesized compounds was done using LCMS spectrometer was involved in $^1$H NMR and $^{13}$C NMR spectra in DMSO-$d_6$ with solvent peak as internal standard. IR Spectra was also investigated for the synthesized compounds with the help of Perkin Elmer Spectrum-GX spectrophotometer.

**Synthesis of 3-methyl-1-phenyl-1*H*-pyrazole-5-one (3a-d):** The starting compound 3-methyl-1-phenyl-1*H*-pyrazole-5-one (**3a-d**) was synthesized by refluxing an equimolar mixture of phenylhydrazine and ethylacetoacetate along with glacial acetic acid in a water bath for almost 1.5 h at 70-75 ºC. After the completion of the reaction, the mixture was brought to room temperature and then kept in an ice-bath. To a mixture ether was added slowly with constant stirring when the precipitates got separated. The precipitated compound was filtered and washed to remove any impurities and recrystallization was done using ethanol. The formation of the product was confirmed by TLC.

**Synthesis of 3-methyl-1-phenyl-5-chloro-1*H*-pyrazole-4-carbaldehyde (4a-d):** 3-Methyl-1-phenyl-1*H*-pyrazole-5-one (**3a-d**) was then converted to 3-methyl-1-phenyl-5-chloro-1*H*-pyrazole-4-carbaldehyde (**4a-d**) using the VMH reaction where equimolar amount of $POCl_3$ (0.4 mol) was added dropwise to an ice-cold DMF (0.4 mol) slowly with continuous stirring. Once the addition was complete the stirring was further carried out for almost 45 min for the completed generation of iminium salt. The iminium salt was then refluxed for 5 h at 90 ºC with 3-methyl-1-phenyl-1*H*-pyrazole-5-one (**3a-d**). The refluxed compound after coming to room temperature was then poured on crushed ice when precipitates of 3-methyl-1-phenyl-5-chloro-1*H*-pyrazole-4-carbaldehyde (**4a-d**) separates out. The precipitates were filtered and washed with water to remove all acidic impurities and then recrystallized with ethanol. The overall yield of the reaction was 70-75%.

**Synthesis of 5-(1*H*-imidazol-1-yl)-3-methyl-1-phenyl-1*H*-pyrazole-4-carbaldehyde (6a-d):** The aldehyde compound 5-(1*H*-imidazol-1-yl)-3-methyl-1-phenyl-1*H*-pyrazole-4-carbaldehyde (**6a-d**) was synthesized by simply refluxing 3-methyl-1-phenyl-5-chloro-1*H*-pyrazole-4-carbaldehyde (**4a-d**) with imidazole (**5**) for 2 h at 85 ºC in presence of anhydrous $K_2CO_3$ as a base catalyst and DMF as a solvent. To isolate 5-(1*H*-imidazol-1-yl)-3-methyl-1-phenyl-1*H*-pyrazole-4-carbaldehyde (**6a-d**), the reaction mixture was cooled to room temperature, poured onto ice water and stirred constantly until the precipitate formed. It was a nucleophilic substitution of the chloro group by imidazole. The crude product was filtered, washed with water and recrystallized with ethanol with an overall yield of 67-70%.

**Synthesis of target molecule 4-(5-(1*H*-imidazol-1-yl)-3-methyl-1-phenyl-1*H*-pyrazol-4-yl)-6-amino-3-methyl-1-phenyl-1,4-dihydropyrano[2,3-*c*]pyrazole-5-carbonitrile (9a-h):** Target molecules **9a-h** were synthesized using the one pot multi-component reaction approach. For this calculated amount of the reaction mixture consisting of 5-(1*H*-imidazol-1-yl)-3-methyl-1-phenyl-1*H*-pyrazole-4-carbaldehyde (**6a-d**), 2-amino acetonitrile (**7**) and 5-methyl-2-phenyl-2,4-dihydro-3*H*-pyrazol-3-one (**8a-b**) was refluxed for 3-4 h using ethanol as a solvent and pyridine in catalytic amount was added to the round bottom flask. After the reaction was completed, the reaction mixture was brought to room temperature when the crude product separated out and washed finally with ethanol to obtain the pure form (**Scheme-I**).

**4-(5-(1*H*-Imidazol-1-yl)-3-methyl-1-phenyl-1*H*-pyrazol-4-yl)-6-amino-3-methyl-1-phenyl-1,4-dihydropyrano[2,3-*c*]-pyrazole-5-carbonitrile (9a):** . Yield: 85%. IR (KBr, $\nu_{max}$, cm$^{-1}$): 3320 and 3075 (asym. and sym. *str*. -$NH_2$), 2140 (-C≡N *str.*). $^1$H NMR (400 MHz, DMSO-$d_6$) δ ppm: 1.82, 1.89 (s, 3H, 2 × $CH_3$), 4.76 (s, 1H, H4), 8.41 (s, 2H, $NH_2$), 6.73-7.90 (m, 13H, Ar-H). $^{13}$C NMR (400 MHz, DMSO-$d_6$) δ ppm: 13.82, 14.10 ($CH_3$), 26.42 (C4), 57.56 (C-CN), 97.93, 108.18, 114.35, 118.30, 119.56, 120.24, 121.00, 125.31, 130.00, 130.71, 132.45, 132.97, 135.56, 137.34, 145.25, 146.15, 147.74, 155.21, 160.83 (Ar-C). MS (*m/z*): 474.1 ($M^+$). Anal. calcd. (found) % for $C_{27}H_{22}N_8O$ (*m.w.* 474.53): C, 68.34 (68.17); H, 4.67 (4.83); O, 3.37 (3.49); N, 23.61 (23.47)

**4-(5-(1*H*-Imidazol-1-yl)-3-methyl-1-(*p*-tolyl)-1*H*-pyrazol-4-yl)-6-amino-3-methyl-1-phenyl-1,4-dihydropyrano[2,3-*c*]-pyrazole-5-carbonitrile (9b):** Yield: 82%. IR (KBr, $\nu_{max}$, cm$^{-1}$): 3345 and 3090 (asym. and sym. *str.* -$NH_2$), 2115 (-C≡N *str.*). $^1$H NMR (400 MHz, DMSO-$d_6$) δ ppm: 1.92, 1.98, 2.41 (s, 3H, 3×$CH_3$), 4.64 (s, 1H, H4), 8.38 (s, 2H, $NH_2$), 6.78-7.72 (m, 12H, Ar-H). $^{13}$C NMR spectrum (400 MHz, DMSO-$d_6$) δ ppm: 13.71, 14.15, 21.18 ($CH_3$), 26.27 (C4), 57.10 (C-CN), 96.98, 109.11, 115.50, 118.82, 119.00, 120.54, 121.77, 126.43, 130.07, 130.67, 132.12, 132.92, 135.38, 137.08, 145.43, 145.99, 147.14, 154.25, 160.34 (Ar-C). MS (*m/z*): 488.2 ($M^+$). Anal. calcd. (found) % for $C_{28}H_{24}N_8O$ (*m.w.* 488.56): C, 68.84 (68.71); H, 4.95 (4.77); O, 3.27 (3.45); N, 22.94 (23.07).

**4-(5-(1*H*-Imidazol-1-yl)-1-(4-methoxyphenyl)-3-methyl-1*H*-pyrazol-4-yl)-6-amino-3-methyl-1-phenyl-1,4-dihydropyrano[2,3-*c*]pyrazole-5-carbonitrile (9c):** Yield: 79%. IR (KBr, $\nu_{max}$, cm$^{-1}$): 3350 and 3060 (asym. and sym. *str.* of -$NH_2$), 2135 (-C≡N *str.*). $^1$H NMR (400 MHz, DMSO-$d_6$) δ ppm: 1.80, 1.86 (s, 3H, 2×$CH_3$), 3.72 (s, 3H, $OCH_3$),4.71 (s, 1H, H4), 8.47 (s, 2H, $NH_2$), 6.83-7.78 (m, 12H, Ar-H). $^{13}$C NMR (400 MHz, DMSO-$d_6$) δ ppm: 13.86, 14.08 ($CH_3$), 26.54 (C4), 54.05 ($OCH_3$), 57.90 (C-CN), 97.10, 108.88, 113.00, 118.64, 119.30, 120.34, 122.05, 125.56, 130.21, 131.11, 132.20, 133.00, 135.15, 137.56, 145.51, 146.26, 147.34, 155.71, 160.41 (Ar-C). MS (*m/z*): 504.2 ($M^+$). Anal. calcd. (found) % for $C_{28}H_{24}N_8O_2$ (*m.w.* 504.55): C, 66.65 (66.79); H, 4.79 (4.65); O, 6.34 (6.53); N, 22.21 (22.43).

**6-Amino-4-(1-(4-chlorophenyl)-5-(1*H*-imidazol-1-yl)-3-methyl-1*H*-pyrazol-4-yl)-3-methyl-1-phenyl-1,4-dihydro-pyrano[2,3-*c*]pyrazole-5-carbonitrile (9d):** Yield: 75%. IR (KBr, $\nu_{max}$, cm$^{-1}$): 3335 and 3070 (asym. and sym. *str*. -$NH_2$), 2120 (-C≡N *str.*),718 (C-Cl *str.*). $^1$H NMR (400 MHz, DMSO-$d_6$) δ ppm: 1.80, 1.89 (s, 3H, 2×$CH_3$), 4.82 (s, 1H, H4), 8.52

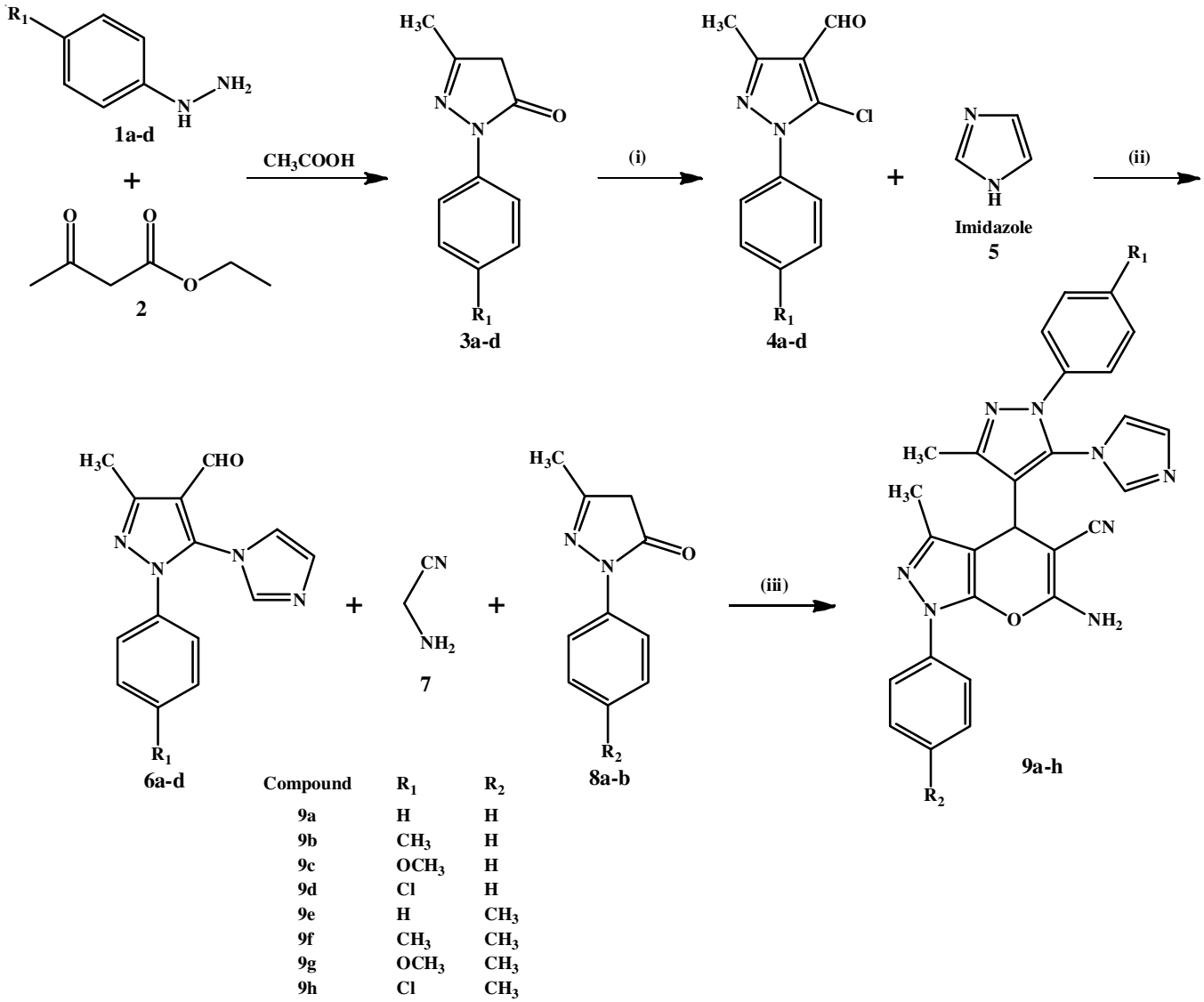


| Compound | $R_1$ | $R_2$ |
|---|---|---|
| 9a | H | H |
| 9b | $CH_3$ | H |
| 9c | $OCH_3$ | H |
| 9d | Cl | H |
| 9e | H | $CH_3$ |
| 9f | $CH_3$ | $CH_3$ |
| 9g | $OCH_3$ | $CH_3$ |
| 9h | Cl | $CH_3$ |

**Scheme-I:** Synthesis of compounds **9a-h** (Reagents and conditions: (i) DMF, $POCl_3$, reflux; (ii) DMF, $K_2CO_3$, reflux; (iii) EtOH, piperidine, reflux

(s, 2H, $NH_2$), 6.90-7.81 (m, 12H, Ar-H). $^{13}$C NMR (400 MHz, DMSO-$d_6$) δ ppm: 13.87, 14.09 ($CH_3$), 26.48 (C4), 57.51 (C-CN), 97.00, 108.45, 115.12, 118.37, 119.10, 120.55, 121.56, 125.74, 130.27, 131.00, 132.60, 133.16, 135.74, 137.40, 145.45, 146.67, 147.40, 155.30, 160.23 (Ar-C). MS (*m/z*): 508.1 ($M^+$). Anal. calcd. (found) % for $C_{27}H_{21}N_8OCl$ (*m.w.* 508.97): C, 63.72 (68.84); H, 4.16 (4.23); Cl, 6.97 (6.72); O, 3.14 (3.24); N, 22.02 (21.97).

**4-(5-(1*H*-Imidazol-1-yl)-3-methyl-1-phenyl-1*H*-pyrazol-4-yl)-6-amino-3-methyl-1-(*p*-tolyl)-1,4-dihydropyrano[2,3-*c*]-pyrazole-5-carbonitrile (9e):** Yield: 83%. IR (KBr, $\nu_{max}$, $cm^{-1}$): 3320 and 3085 (asym. and sym. *str.* -$NH_2$), 2145 (-C≡N *str.*). $^1$H NMR (400 MHz, DMSO-$d_6$) δ ppm: 1.84, 1.92, 2.40 (s, 3H, 3×$CH_3$), 4.76 (s, 1H, H4), 8.42 (s, 2H, $NH_2$), 6.82-7.78 (m, 12H, Ar-H). $^{13}$C NMR (400 MHz, DMSO-$d_6$) δ ppm: 13.86, 14.18, 21.24 ($CH_3$), 26.28 (C4), 57.44 (C-CN), 97.32, 109.56, 115.11, 118.56, 119.20, 120.43, 121.57, 126.35, 130.64, 131.14, 132.78, 133.46, 136.00, 137.45 145.72, 146.34, 147.65, 154.90, 160.38 (Ar-C). MS (*m/z*): 488.2 ($M^+$). Anal. calcd. (found) % for $C_{28}H_{24}N_8O$ (*m.w.* 488.56): C, 68.84 (69.02); H, 4.95 (5.12); O, 3.27 (3.39); N, 22.94 (22.73).

**4-(5-(1*H*-Imidazol-1-yl)-3-methyl-1-(*p*-tolyl)-1*H*-pyrazol-4-yl)-6-amino-3-methyl-1-(*p*-tolyl)-1,4-dihydropyrano[2,3-*c*]-pyrazole-5-carbonitrile (9f):** Yield: 78%. IR (KBr, $\nu_{max}$, $cm^{-1}$): 3340 and 3075 (asym. and sym. *str.* -$NH_2$), 2130 (-C≡N *str.*). $^1$H NMR (400 MHz, DMSO-$d_6$) δ ppm: 1.90, 1.96, 2.38, 2.46 (s, 3H, 4×$CH_3$), 4.72 (s, 1H, H4), 8.50 (s, 2H, $NH_2$), 6.88-7.80 (m, 11H, Ar-H). $^{13}$C NMR (400 MHz, DMSO-$d_6$) δ ppm: 13.82, 14.11, 21.14, 21.22 ($CH_3$), 26.21 (C4), 57.43 (C-CN), 97.12, 109.35, 115.21, 118.24, 119.45, 120.00, 121.70, 126.34, 130.45, 130.98, 132.60, 133.12, 135.88, 137.75 145.60, 146.12, 147.78, 154.45, 160.65 (Ar-C). MS (*m/z*): 502.2 ($M^+$). Anal. calcd. (found) % for $C_{29}H_{26}N_8O$ (*m.w.* 502.58): C, 69.31 (69.20); H, 5.21 (4.97); O, 3.18 (3.35); N, 22.30 (22.48).

**4-(5-(1*H*-Imidazol-1-yl)-1-(4-methoxyphenyl)-3-methyl-1*H*-pyrazol-4-yl)-6-amino-3-methyl-1-(*p*-tolyl)-1,4-dihydropyrano[2,3-*c*]pyrazole-5-carbonitrile (9g):** Yield: 82%. IR (KBr, $\nu_{max}$, $cm^{-1}$): 3345 and 3015 (asym. and sym. *str.*

-$NH_2$), 2160 (-C≡N *str.*). $^1$H NMR (400 MHz, DMSO-$d_6$) δ ppm: 1.88, 1.90, 2.42 (s, 3H, 3×$CH_3$), 3.75 (s, 3H, $OCH_3$), 4.68 (s, 1H, H4), 8.43 (s, 2H, $NH_2$), 6.88-7.76 (m, 11H, Ar-H). $^{13}$C NMR (400 MHz, DMSO-$d_6$) δ ppm: 13.90, 14.13, 21.25 ($CH_3$), 26.40 (C4), 54.25 ($OCH_3$), 57.83 (C-CN), 98.15, 110.20, 114.15, 118.00, 119.75, 120.70, 122.30, 126.16, 130.50, 131.61, 132.20, 134.20, 135.65, 137.20, 145.70, 146.26, 148.10, 155.70, 160.23 (Ar-C). MS (*m/z*): 518.2 ($M^+$). Anal. calcd. (found) % for $C_{29}H_{26}N_8O_2$ (*m.w.* 518.58): C, 67.17 (66.94); H, 5.05 (5.12); O, 6.17 (6.34); N, 21.61 (21.46).

**6-Amino-4-(1-(4-chlorophenyl)-5-(1*H*-imidazol-1-yl)-3-methyl-1*H*-pyrazol-4-yl)-3-methyl-1-(*p*-tolyl)-1,4-dihydropyrano[2,3-*c*]pyrazole-5-carbonitrile (9h):** Yield: 85%. IR (KBr, $\nu_{max}$, $cm^{-1}$): 3360 and 3055 (asym. and sym. *str.* -$NH_2$), 2135 (-C≡N *str.*), 718 (C-Cl *str.*). $^1$H NMR (400 MHz, DMSO-$d_6$) δ ppm: 1.82, 1.87, 2.38 (s, 3H, 3×$CH_3$), 4.86 (s, 1H, H4), 8.58 (s, 2H, $NH_2$), 6.84-7.76 (m, 11H, Ar-H). $^{13}$C NMR (400 MHz, DMSO-$d_6$) δ ppm: 14.24, 15.12, 22.10 ($CH_3$), 26.15 (C4), 58.04 (C-CN), 98.12, 107.95, 115.12, 117.20, 119.45, 120.34, 122.13, 125.36, 130.68, 131.35, 132.87, 133.65, 135.14, 138.55, 145.67, 146.80, 148.15, 155.72, 160.45 (Ar-C). MS (*m/z*): 522.1 ($M^+$). Anal. calcd. (found) % for $C_{28}H_{23}N_8OCl$ (*m.w.* 523.00): C, 64.30 (64.44); H, 4.43 (4.23); Cl, 6.78 (6.60); O, 3.06 (3.21); N, 21.43 (21.31).

### Computational studies

**Density functional theory:** All the synthesized structures were optimized to obtain the lowest possible energy level using quantum computational tool ORCA 5.0.3 with DFT method and B3LYP level of DFT theory and def-2SVP basis set [19]. The structure obtained with the lowest possible energy was then checked for any negative vibrational frequency in IR range computationally with same parameters as used in case of optimization, finding no such negative frequency confirmed the acceptable geometry of compound at lowest single point energy. This study was carried out to understand the influence of change in substitution groups at $R_1$ and $R_2$ positions. The angle between the core rings of the molecule as well as distribution of the charge over the molecule as on individual atoms and their molecular orbital responsible for electronic properties of the molecule as they are good indicators of electron transport in the system, responsible for UV-vis properties of the molecule. Four planes were passed from the molecule in order to understand the effect of substitutions, where two planes were passed from pyrazole rings and other two planes were passed from phenyl pyrazole rings. The angle between the $R_1$ substituted phenyl pyrazole and pyrazole ring was noted as twist angle $\theta_1$, the angle between the $R_2$ substituted phenyl pyrazole and pyrazole ring was observed as twist angle $\theta_2$, the angle between two pyrazole ring was noted as twist angle $\theta_3$ and the angle between two substituted phenyl pyrazole ring was noted as twist angle $\theta_4$.

### Molecular docking study

**With EGFR:** To get the understanding of the behaviour of the particular pharmacophore and their potency to guide the SAR, the interaction of the synthesized compounds with EGFR (PDB code: 1M17) was examined by docking the protein and ligand molecules into the active pocket of the protein. The protein structure was corrected for any structural error using homology model preparation and protonation of the molecule with partial charge into MOE software. The prepared ligand molecules were then docked at the ligand site with induced fit refinement.

**With FabH:** Similarly, to get the understanding of the behaviour of the particular pharmacophore and their potency to guide the SAR, molecular docking of compounds and *E. coli* FabH was performed and examined on the binding model based on *E. coli* FabH-CoA complex structure (PDB code: 1HNJ).

## RESULTS AND DISCUSSION

The IR spectra was carried out for all the eight synthesized compounds **9a-h** in order to confirm the type of functional groups present in them. The symmetric and asymmetric stretching bands of the primary amine (-$NH_2$) were observed in the region of 3090-3015 and 3350-3320 $cm^{-1}$ for compounds **9a-h**. The stretching bands for cyanide (-CN) group in compounds **9a-h** appeared in the range of 2160-2115 $cm^{-1}$. A C-Cl stretching was observed for compounds **9d** and **9h** in the 718 $cm^{-1}$ region.

$^1$H NMR was carried out to confirm the structure of all the eight synthesized compounds **9a-h**. A singlet for three protons each in two different methyl groups was observed in the region of δ 1.80-1.98 ppm for all the compounds **7a-h** whereas in compounds **9b**, **9e**, **9g** and **9h** a singlet for third methyl group as $R_1$ substitution and in compound **9f** a singlet for fourth methyl group as $R_2$ substitution with three protons appeared in the region of δ 2.38-2.42 ppm. Three protons as $R_2$ substitute of methoxy group in compounds **9c** and **9g** resonated in the region of δ 3.72-3.75 ppm. An aromatic chiral proton for all the synthesized compounds **9a-h** was observed in the region of δ 4.64-4.86 ppm as a singlet. A multiplet for aromatic protons ranging from eleven to thirteen in compounds **9a-h** appeared in the region of δ 6.73-7.90 ppm. A singlet for two protons of the amino group in all the synthesized compounds **9a-h** was observed in the range of δ 6.38-6.58 ppm.

All the synthesized compounds (**9a-h**) were analyzed for their $^{13}$C NMR absorption spectra. The two methyl groups present on the pyrazole ring and pyrano-pyrazole ring of all synthesized compounds **9a-h** showed signals in the range of δ 13.71-14.24 ppm and 14.09-15.12 ppm, respectively. A methyl group substitution at $R_1$ in compounds **9b** and **9f** and $R_2$ substitution in compounds **9e-h** gave signals in the range of δ 21.14-22.10 ppm. Active methylene (C4) displayed a single line in the range of δ 26.15-26.54 ppm for compounds **9a-h**. The presence of a nitrile carbon atom in all eight compounds **9a-h** was confirmed by a single peak at δ 57.10-58.04 ppm. A methoxy group substitution at $R_1$ in compounds **9c** and **9g** was confirmed by a single line in the range of δ 54.05-54.25 ppm. A multiplet of aromatic carbon atoms for compounds **9a-h** was confirmed in the range of δ 97-160.83 ppm.

### Biological evaluation

**Antiproliferation and EGFR inhibitory activity:** All the synthesized eight compounds having two phenyl pyrazole

groups with various substitution matrix were tested for EGFR inhibitory activity as well as antiproliferation activity against known lung cancer cell line A549 known as adenocarcinoma human alveolar basal epithelial cell line and liver cancer cell line Hep G2. In case of EGFR inhibition, the mode of action to inhibit tyrosine kinase is well known, by stopping the transferring of signal between the two EGFR molecules. When the synthesized molecules were tested for these activities, it was found that compound **9g** showed most potent activity amongst the synthesized compounds with $IC_{50}$ of 0.11 ± 0.02 μM, while compounds **9d** and **9a** showed compared good activity with $IC_{50}$ of 0.18 ± 0.06 μM and $IC_{50}$ of 0.21 ± 0.04 μM, respectively. In case of antiproliferative activity against A549 and Hep G2 compound **9d** showed most potent activity with $IC_{50}$ of 1.21 ± 0.05 μM and 1.96 ± 0.03 μM, respectively, whereas compound **9e** showed potency against the A549 with $IC_{50}$ of 1.52 ± 0.11 μM and compound **9d** showed potency against the Hep G2 with $IC_{50}$ of 2.84 ± 0.11 μM, although among all the synthesized compounds only compound **9d** showed the nearest potency compared to the standard erlotinib.

***E. coli* FabH inhibitory activity:** The *E. coli* FabH inhibitory activity of the synthesized eight compounds **9a-h** were examined and their result as a concentration in micro mole is represented in Table-1. Among eight compounds, three of them showed a fair inhibitory activity. Compound **9h** showed the most potent inhibitory activity with the $IC_{50}$ of 2.6 μM, while compound **9a** showed inhibitory action at the $IC_{50}$ of 3.2 μM and compound **9g** showed inhibitory action at the $IC_{50}$ of 5.4 μM. While the other derivatives **9b**, **9c**, **9d**, **9e** and **9f** showed the inhibitory action at the $IC_{50}$ of 14.2 μM, 12.7 μM, 6.3 μM, 10.2 μM and 15.4 μM, respectively.

## Computational studies

**Density functional theory:** It has been generally accepted that materials will be more reactive and less kinetically stable the smaller the molecular orbital energy gap ΔE [20,21], However, recent research has shown that this conventional relationship is not always followed [22]. The theoretical values of the energy gap of molecular orbital obtained from DFT study is represented in Table-2. The molecular surface plot of all the prepared molecules is represented in Fig. 1. It can be observed that in molecules **9a** and **9g** the HOMO density is spread over the center of the molecule indicating easy mobility of electron around the center enhancing inter molecular charge transfer while LUMO is delocalized over the whole $R_1$ phenyl pyrazole fraction of the molecule, in molecule **9b** and **9c**, the HOMO

TABLE-1
INHIBITION OF EGFR KINASE, ANTIPROLIFERATIVE AND *E. coli* FabH INHIBITORY ACTIVITY $IC_{50}$ (μM) DATA OF COMPOUNDS **9a-h**

| Compound | EGFR | A549 | Hep G2 | *E. coli* FabH $IC_{50}$ (μM) | Hemolysis LC30[a] (mg/mL) |
|---|---|---|---|---|---|
| **9a** | 0.21 ± 0.04 | 2.10 ± 0.06 | 2.46 ± 0.05 | 3.2 | > 10 |
| **9b** | 1.21 ± 0.03 | 6.55 ± 0.24 | 7.27 ± 0.10 | 14.2 | > 10 |
| **9c** | 2.33 ± 0.19 | 8.57 ± 0.31 | 9.26 ± 0.17 | 12.7 | > 10 |
| **9d** | 0.18 ± 0.06 | 3.36 ± 0.10 | 2.84 ± 0.11 | 6.3 | > 10 |
| **9e** | 3.63 ± 0.14 | 1.52 ± 0.11 | 3.10 ± 0.14 | 10.2 | > 10 |
| **9f** | 0.90 ± 0.05 | 2.60 ± 0.15 | 4.88 ± 0.12 | 15.4 | > 10 |
| **9g** | 0.11 ± 0.02 | 1.21 ± 0.05 | 1.96 ± 0.03 | 5.4 | > 10 |
| **9h** | 4.03 ± 0.26 | 6.39 ± 0.14 | 7.37 ± 0.13 | 2.6 | > 10 |
| Erlotinib | 0.032 ± 0.02 | 0.13 ± 0.01 | 0.12 | [a]Lytic concentration 30% | |

TABLE-2
FACTORS CALCULATED FROM THE QUANTUM COMPUTATIONAL DFT STUDY OF MOST AND LEAST ACTIVE MOLECULES

| Element | | **9a** | **9b** | **9c** | **9d** | **9e** | **9f** | **9g** | **9h** |
|---|---|---|---|---|---|---|---|---|---|
| Dipole moment (Debye) | | 3.720 | 3.301 | 3.856 | 5.165 | 4.267 | 3.755 | 4.230 | 5.782 |
| Energy (a.u.) | | -1555.624 | -1594.883 | -1670.000 | -2015.027 | -1594.883 | -1634.142 | -1709.259 | -2054.286 |
| Twist angle (θ) | $\theta_1$ | 20.65 | 18.67 | 19.84 | 15.14 | 14.93 | 15.17 | 17.46 | 15.18 |
| | $\theta_2$ | 17.00 | 7.02 | 6.91 | 9.16 | 12.36 | 11.08 | 10.71 | 13.08 |
| | $\theta_3$ | 63.40 | 70.47 | 71.46 | 68.60 | 64.90 | 67.63 | 70.04 | 64.07 |
| | $\theta_4$ | 63.90 | 70.20 | 70.68 | 70.17 | 68.93 | 68.22 | 68.88 | 67.81 |
| $E_{HOMO}$ (eV) | | -2.867 | -8.738 | -8.749 | -2.861 | -5.470 | -2.870 | -6.394 | -2.861 |
| $E_{LUMO}$ (eV) | | -1.473 | -2.149 | -1.749 | -1.092 | -1.451 | -1.166 | -1.090 | -1.090 |
| $I = -E_{HOMO}$ | | 2.867 | 8.738 | 8.749 | 2.861 | 5.470 | 2.870 | 6.394 | 2.861 |
| $A = -E_{LUMO}$ | | 1.473 | 2.149 | 1.749 | 1.092 | 1.451 | 1.166 | 1.090 | 1.090 |
| $\Delta E = I - A$ (eV) | | 1.394 | 6.589 | 7.000 | 1.769 | 4.019 | 1.704 | 5.304 | 1.771 |
| $\eta = (I - A)/2$ | | 0.697 | 3.295 | 3.500 | 0.885 | 2.010 | 0.852 | 2.652 | 0.886 |
| $\chi = (I + A)/2$ | | 2.170 | 5.444 | 5.249 | 1.977 | 3.461 | 2.018 | 3.742 | 1.976 |
| $\sigma = 1/\eta$ | | 1.435 | 0.304 | 0.286 | 1.131 | 0.498 | 1.174 | 0.377 | 1.129 |
| $S = 1/2\eta$ | | 0.717 | 0.152 | 0.143 | 0.565 | 0.249 | 0.587 | 0.189 | 0.565 |
| $Pi = -\chi$ | | -2.170 | -5.444 | -5.249 | -1.977 | -3.461 | -2.018 | -3.742 | -1.976 |
| $\omega = (Pi)^2/2\eta$ | | 3.378 | 4.497 | 3.936 | 2.208 | 2.980 | 2.390 | 2.640 | 2.204 |
| $\Delta N_{max} = \chi/\eta$ | | 3.113 | 1.652 | 1.500 | 2.235 | 1.722 | 2.369 | 1.411 | 2.231 |

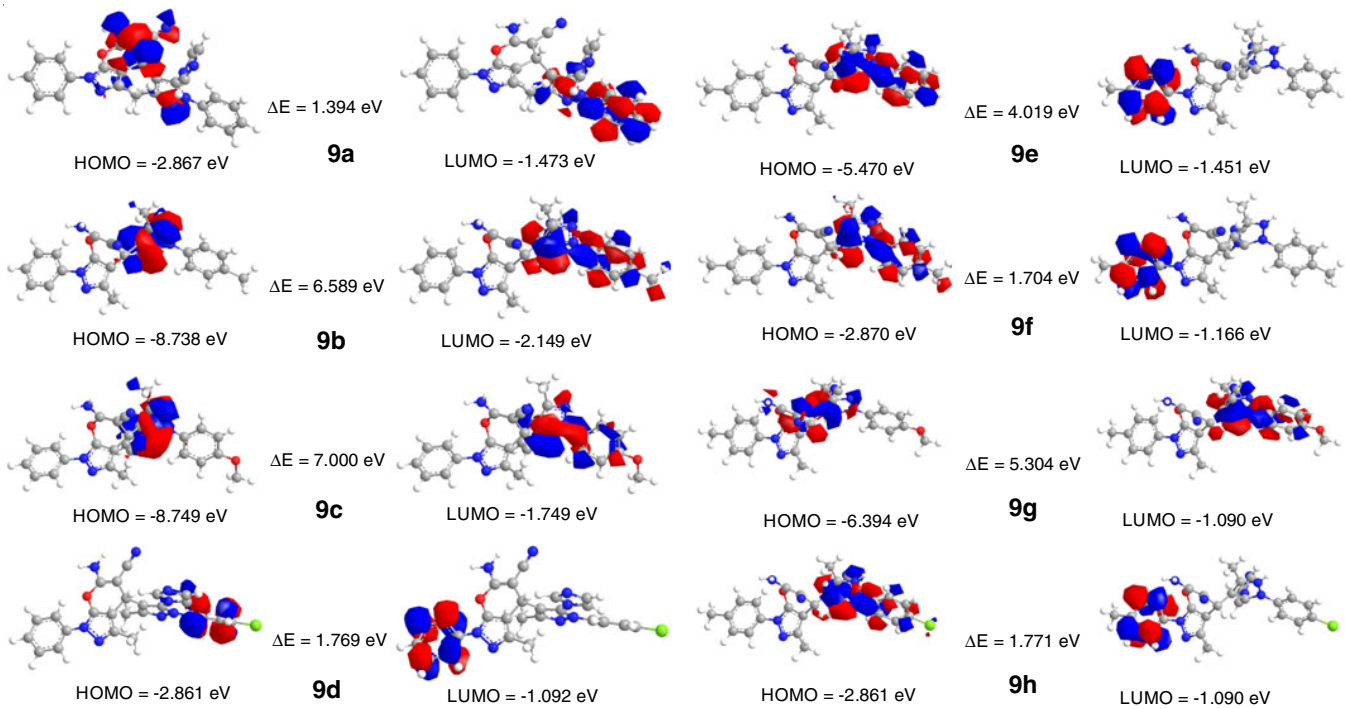


Fig. 1. Frontier molecular orbitals diagram of **9a-h**

density is localized over $R_1$ pyrazole ring and LUMO is delocalized over the $R_1$ phenyl pyrazole fraction of molecule, in **9d** molecule HOMO density is localized over $R_1$ phenyl ring and LUMO is localized over $R_2$ phenyl ring, this localization of density over phenyl ring indicating favourable atomic center within phenyl rings for possible nucleophilic attack. In molecules **9e**, **9f** and **9h** the HOMO density is delocalized over the $R_1$ phenyl pyrazole fragment of the molecule and LUMO is localized over on $R_2$ phenyl ring. Other parameters based on the molecular orbital energy level gap are the softness, hardness, global softness, absolute softness, chemical potential, global electrophilicity, electronegativity and additional electronic charge are reported in Table-2 with the molecular energy, twist angles between planes and dipole moment. It is clear that the correlation between molecule softness and reactivity does not hold, hence this kind of information on its own is insufficient to account for molecule reactivity.

**Molecular docking study:** From the inhibition concentration data of EGFR kinase inhibition and antiproliferative activities it was observed that among all the prepared compounds, compound **9g** exhibited greater potency against all three cancer cell lines, which are EGFR, A549 and HepG2 with the $IC_{50}$ of 0.11 ± 0.02, 1.21 ± 0.05 and 1.96 ± 0.03, respectively. Compound **9h** showed least activity against the EGFR with $IC_{50}$ of 4.03 ± 0.26, while compound **9c** showed the least activity against A549 cell line and HepG2 $IC_{50}$ of 8.57 ± 0.31 and 9.26 ± 0.17, this can be attributed to the electron donating and electron withdrawing groups at the $R_2$ position as they are of opposite character and can affect the molecular orbital localization at the $R_2$ phenyl group as well as localization of occupied orbital density over the core. This change in substitution bring a change in the twist angle between the aromatic part of the molecule allowing the molecule to fit perfectly in the pocket of EFGR, which can be quantitatively seen in Table-2 and qualitatively observed in Fig. 2. A strong interaction of compound **9g** with protein with residues CYS773, ARG817, ASP831 and LYS721, among which former three residues form two hydrogen or one hydrogen and one π hydrogen bond with the binding energy of -9.0233 kcal/mol. These interaction of compound **9g** with protein residues are shown in Fig. 3.

The binding energy of all compounds are summarized in Table-3. It was found that compound **9d** was bound into the active pocket of the EGFR with the minimum binding energy $\Delta G_b$ of -9.2430 kcal/mol, the 2D and 3D binding interaction of compound **9d** is showed in Fig. 4. All the amino acid residues that had interacted with the ligand within the active radius of about 5 Å are labeled. Binding showed that compound **9d** bound in the site of EGFR through hydrophobic interaction. The binding was stabilized by seven hydrogen bonds, among which one hydrogen bond formed between the chlorine at $R_1$ substitution and GLN767 with bond distance of 2.87 Å, second and third hydrogen bond between pyrazolidine nitrogen and LYS721 and pyrazolidine nitrogen and ASP831 with respective bond

TABLE-3
BINDING ENERGIES OF COMPOUNDS **9a-h** HAVING ERLOTINIB WITH EGFR AND MALONYL CoA WITH FabH

| Compound | Binding energy $\Delta G_b$ | |
|---|---|---|
| | EGFR | FabH |
| **9a** | -7.8844 | -6.5140 |
| **9b** | -7.2793 | -8.0856 |
| **9c** | -7.3714 | -7.3044 |
| **9d** | -9.2430 | -7.2489 |
| **9e** | -7.3080 | -7.8391 |
| **9f** | -8.9766 | -5.8785 |
| **9g** | -9.0233 | -5.9469 |
| **9h** | -7.6501 | -8.0110 |

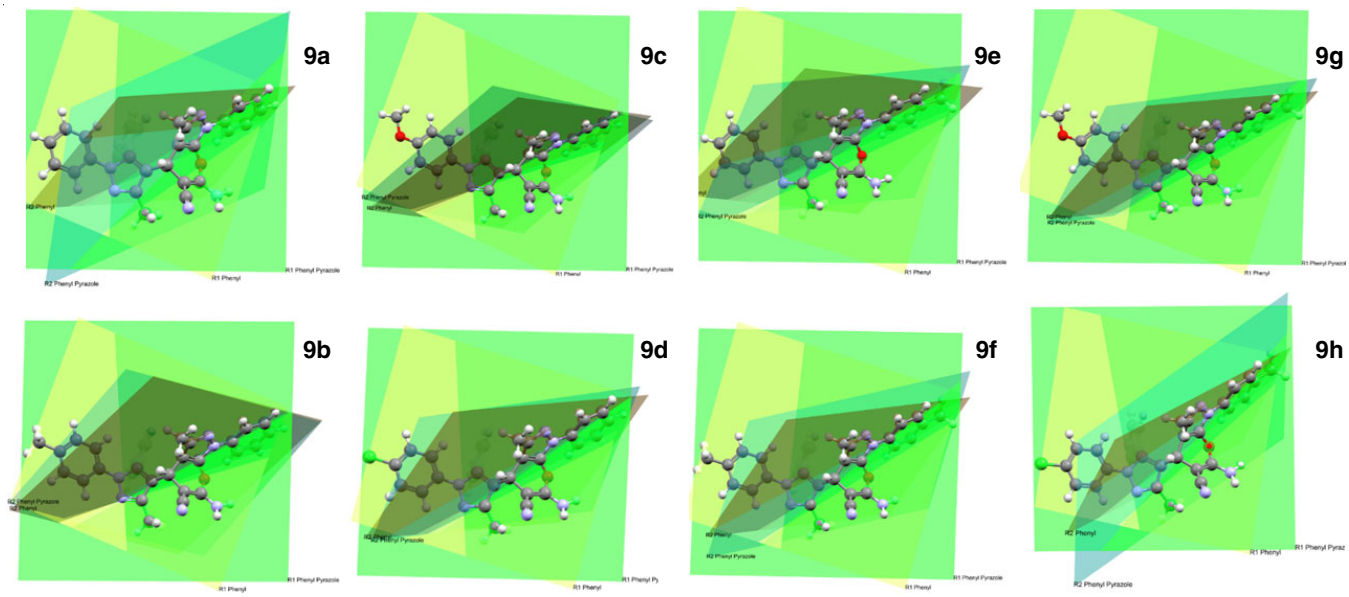


Fig. 2. Twist angle 1 of **9a-h**

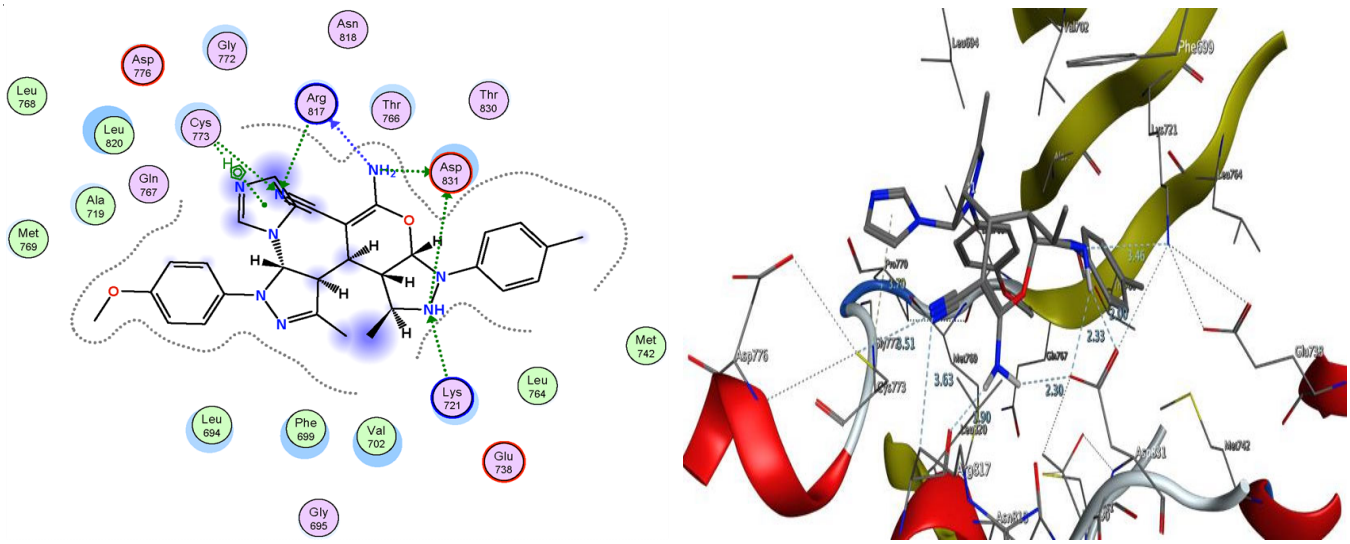


Fig. 3. 2D and 3D Binding model of compound **9g** into the active pocket of EGFR

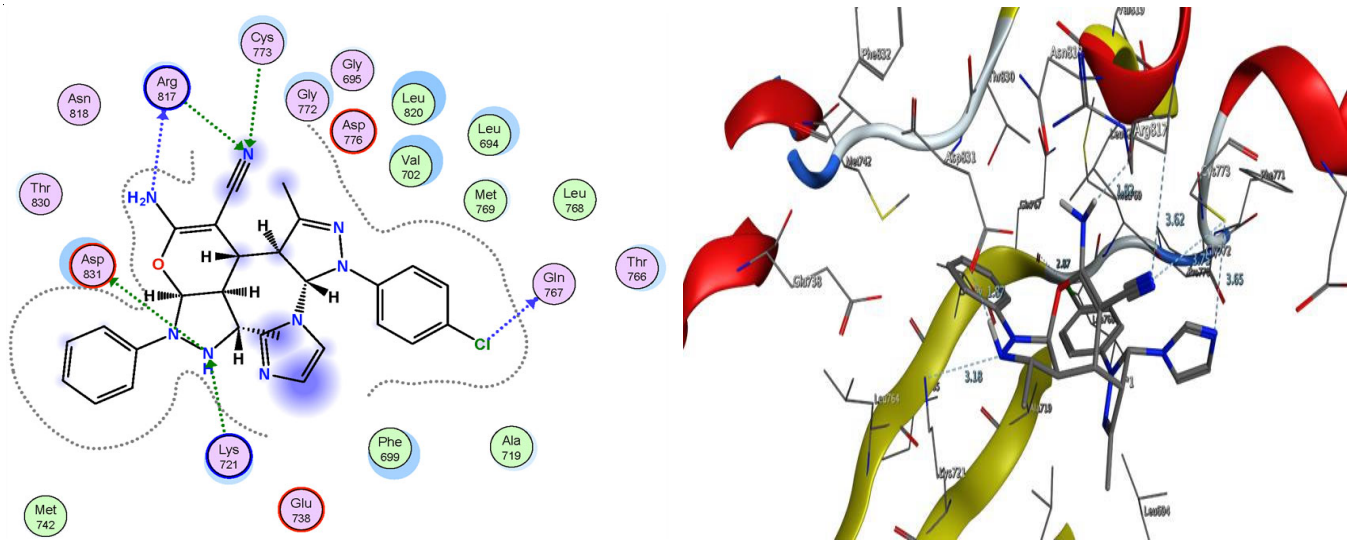


Fig. 4. 2D and 3D Binding model of compound **9d** into the active pocket of EGFR

distance of 3.18 Å and 1.87 Å. Fourth was between the amine nitrogen and ARG817 with distance of 1.82 Å while the fifth and sixth bond was between the nitrogen of the cyanide with ARG817 and CYS773 with respective bond length of 3.62 Å and 3.75 Å and the seventh hydrogen bond was between the CYS773 and nitrogen of the imidazole with bond length of 3.65 Å. From this binding model, it could be concluded that these seven hydrogen bonds from the pyrazole, imidazole as well as cyanide and amine group with the pocket are responsible for the effective EGFR inhibitory of compound **9d**.

From the inhibition concentration data of FabH *E. coli* for all the synthesized compounds, it was observed that among them compound **9h** exhibited greater potency with the $IC_{50}$ concentration of 2.6 µM, while compound **9f** showed the least potency against *E. coli* with the $IC_{50}$ concentration of 15.4 µM, from the docking score it can be seen that compound **9b** bound with the least binding energy with the protein, but among the three binding sites in the docking results, two of them are of receptor exposure, while in the docking result of compound **9h**, there is one strong π–π interaction between the $R_1$ aromatic ring and aromatic ring of residue TRP32 and two π–H bond with residue PHE213 and MET207 as can be seen in Fig. 5 and hence shows a greater activity despite comparative lower binding energy than compound **9b**.

A catalytic triad tunnel composed of Cys-His-Asn is found in the active site of the FabH, which is found in several bacteria. This triad which works as catalysis, plays an important role in the controlling of chain elongation as well as substrate binding and hence the alkyl chain of the CoA is broken at the Cys residue of the triad of FabH, the interaction occurring between the Cys and substrate seems to playing a significant role in the binding of the substrate. From studied eight compounds, compound **9b** was found to be bound strongly into the active pocket of the FabH with the binding energy $\Delta G_b$ of -8.0856 kcal/mol on primary analysis of docking results. Binding affinity score of all the prepared compounds is represented in

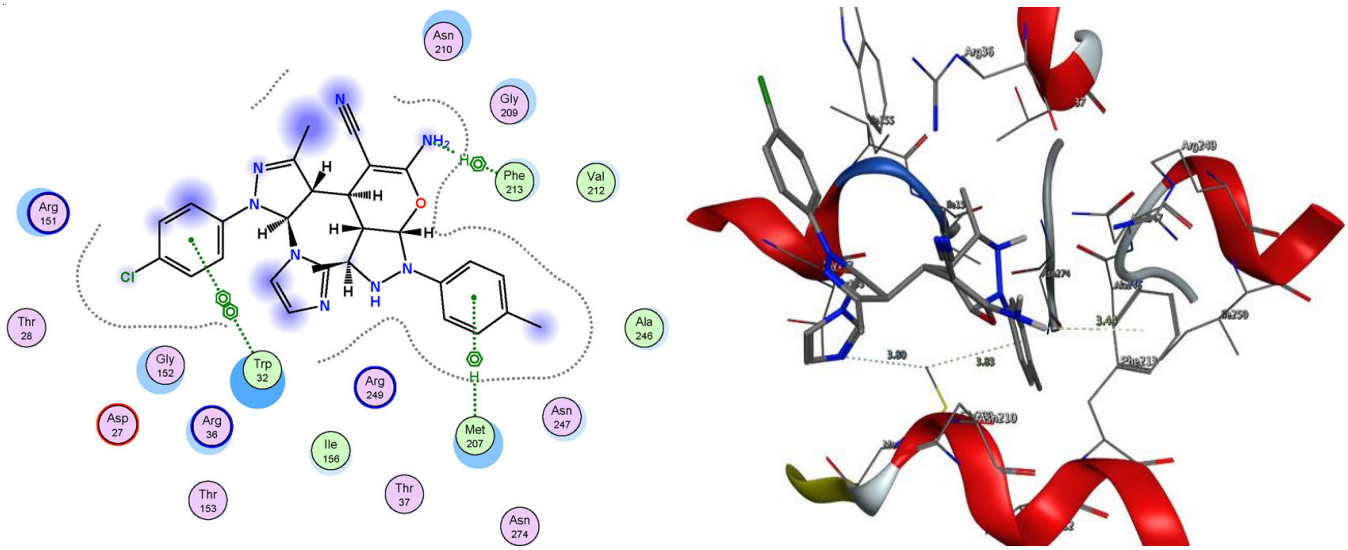


Fig. 5. 2D and 3D Binding model of compound **9h** into the active pocket of FabH

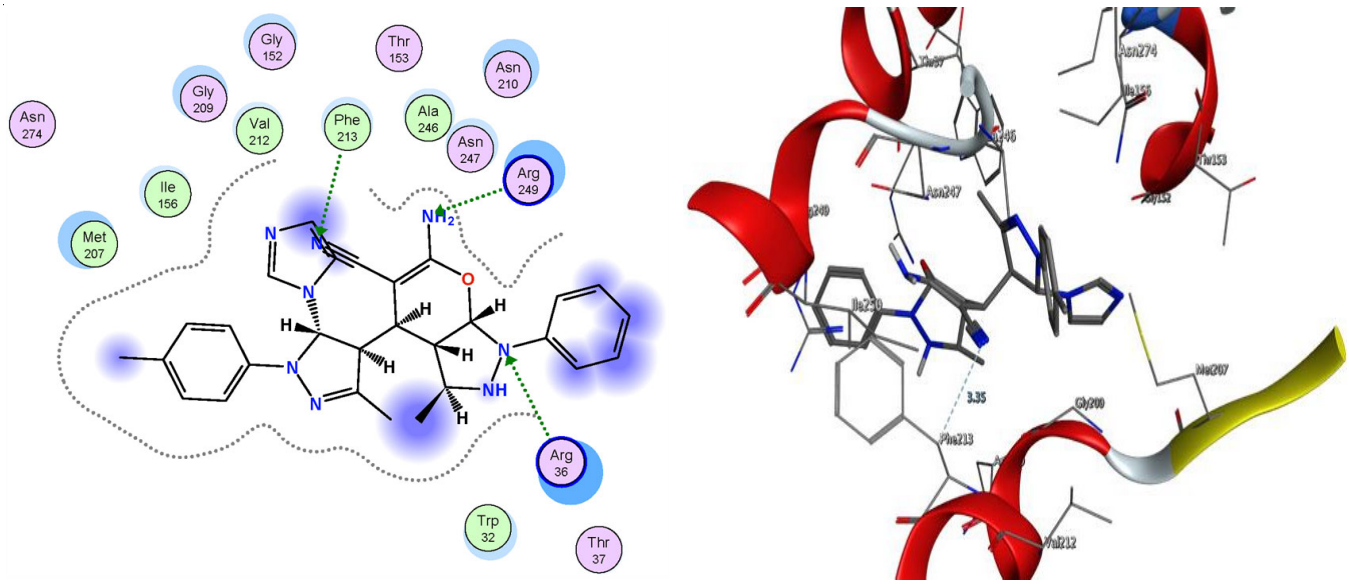


Fig. 6. 2D and 3D Binding model of compound **9b** into the active pocket of FabH

Table-3. The interactive binding model of compound **9b** with the active site of FabH protein in 2D and 3D model is depicted in Fig. 6, respectively. Where it can be seen that in figures that among all three hydrogen bonds, one was formed between cyanide nitrogen and PHE213 with bond distance of 3.35 Å and the other two are strong receptor exposure with amine nitrogen and ARG249 and one between pyrazole nitrogen and ARG36. From this interaction and the binding score, it can be primarily concluded that the strong hydrogen bonding is responsible for the effective FabH inhibitory of compound **9b** in docking results.

## Conclusion

A series of molecule with phenyl pyrazole molecules as a pharmacophore with small substitutions and imidazole as well as primary amine and cyanide groups as potential binding sites is designed and synthesized. Among the prepared compounds, a small but significant number of biological results were obtained, leading us to the conclusion that using the same type of active groups, like phenyl pyrazole as in the present work, increases the probability of binding with greater affinity to the active pocket of the proteins. In current work, compound **9g** was found to be the most active against EGFR, A549 and HepG2, while compound **9h** was found to be most active against FabH *E. coli*, although other members of the synthesized series were also found to be active with comparatively higher inhibition concentration. In addition to the molecular docking, DFT study were also performed to evaluate the distance and angle between the active parts of the molecules as well as distribution of the charge density over the molecule affecting the binding of molecule in the active pocket with greater binding affinity. From this study and observation, it can be concluded that molecules with multiple pharmacophores can be used as templet and can be further engineered for the target-based application, discovering more scope as well as any biological activity limitations.

## ACKNOWLEDGEMENTS

The authors are thankful to Shri Maneklal M. Patel Institute of Sciences and Research, Kadi Sarva Vishwavidhyalaya for giving infrastructure and laboratory facility.

## CONFLICT OF INTEREST

The authors declare that there is no conflict of interests regarding the publication of this article.

## REFERENCES

1. S. Thakral and V. Singh, *Curr. Bioact. Compd.*, **15**, 316 (2019); https://doi.org/10.2174/1573407214666180614121140
2. J.J. Malin and E. de Leeuw, *Infect. Drug Resist.*, **12**, 2613 (2019); https://doi.org/10.2147/IDR.S215070
3. D.R. Giacobbe, M. Mikulska and C. Viscoli, *Expert Rev. Clin. Pharmacol.*, **11**, 1219 (2018); https://doi.org/10.1080/17512433.2018.1549487
4. J. Jampilek, *Molecules*, **24**, 3839 (2019); https://doi.org/10.3390/molecules24213839
5. M. Henary, C. Kananda, L. Rotolo, B. Savino, E.A. Owens and G. Cravotto, *RSC Adv.*, **10**, 14170 (2020); https://doi.org/10.1039/D0RA01378A
6. N. Kerru, L. Gummidi, S. Maddila, K.K. Gangu and S.B. Jonnalagadda, *Molecules*, **25**, 1909 (2020); https://doi.org/10.3390/molecules25081909
7. M. Ramadan, A.A. Aly, L.E.A. El-Haleem, M.B. Alshammari and S. Bräse, *Molecules*, **26**, 4995 (2021); https://doi.org/10.3390/molecules26164995
8. K. Tabassum, P. Ekta and P. Kavitkumar, *Mini-Rev. Org. Chem.*, **15**, 459 (2018); https://doi.org/10.2174/1570193X15666171211170100
9. A. Balbi, M. Anzaldi, C. Macciò, C. Aiello, M. Mazzei, R. Gangemi, P. Castagnola, M. Miele, C. Rosano and M. Viale, *Eur. J. Med. Chem.*, **46**, 5293 (2011); https://doi.org/10.1016/j.ejmech.2011.08.014
10. K. Karrouchi, S. Radi, Y. Ramli, J. Taoufik, Y. Mabkhot, F. Al-aizari and M. Ansar, *Molecules*, **23**, 134 (2018); https://doi.org/10.3390/molecules23010134
11. M. Mantzanidou, E. Pontiki and D. Hadjipavlou-Litina, *Molecules*, **26**, 3439 (2021); https://doi.org/10.3390/molecules26113439
12. D.S. Zinad, A. Mahal and O.A. Shareef, *IOP Conf. Ser.: Mater. Sci. Eng.*, **770**, 012053 (2020); https://doi.org/10.1088/1757-899X/770/1/012053
13. H.A. Abd El Razik, M.H. Badr, A.H. Atta, S.M. Mouneir and M.M. Abu-Serie, *Arch. Pharm.*, **350**, e1700026 (2017); https://doi.org/10.1002/ardp.201700026
14. C.B. Sangani, J.A. Makawana, Y.-T. Duan, Y. Yin, S.B. Teraiya, N.J. Thumar and H.-L. Zhu, *Bioorg. Med. Chem. Lett.*, **24**, 4472 (2014); https://doi.org/10.1016/j.bmcl.2014.07.094
15. J.A. Makawana, C.B. Sangani, L. Lin and H.-L. Zhu, *Bioorg. Med. Chem. Lett.*, **24**, 1734 (2014); https://doi.org/10.1016/j.bmcl.2014.02.041
16. C.B. Sangani, J.A. Makawana, X. Zhang, S.B. Teraiya, L. Lin and H.-L. Zhu, *Bioorg. Med. Chem. Lett.*, **76**, 549 (2014); https://doi.org/10.1016/j.ejmech.2014.01.018
17. C.B. Sangani, H.H. Jardosh, M.P. Patel and R.G. Patel, *Med. Chem. Res.*, **22**, 3035 (2013); https://doi.org/10.1007/s00044-012-0322-5
18. I. Ali, M.N. Lone and H.Y. Aboul-Enein, *MedChemComm*, **8**, 1742 (2017); https://doi.org/10.1039/C7MD00067G
19. F. Neese, *Wiley Interdiscip. Rev. Comput. Mol. Sci.*, **8**, e1327 (2017); https://doi.org/10.1002/wcms.1327
20. R. Kurtaran, S. Odabasioglu, A. Azizoglu, H. Kara and O. Atakol, *Polyhedron*, **26**, 5069 (2007); https://doi.org/10.1016/j.poly.2007.07.021
21. W.H. Mahmoud, M.M. Omar, F.N. Sayed and G.G. Mohamed, *Appl. Organomet. Chem.*, **32**, 4386 (2018); https://doi.org/10.1002/aoc.4386
22. P. Sharma, R. Patel, R.R. Koshti, A. Vyas and C.B. Sangani, *Asian J. Chem.*, **34**, 3169 (2022); https://doi.org/10.14233/ajchem.2022.23981